

Study on the near-surface residual stress state in butt-welded pipes of austenitic steel using X-ray diffraction

Nico Hempel¹  · Thomas Nitschke-Pagel¹ · Klaus Dilger¹

Received: 13 October 2015 / Accepted: 19 August 2016 / Published online: 5 September 2016
© International Institute of Welding 2016

Abstract This study is dedicated to the analysis of the residual stress state of two-pass butt-welded pipes of the austenitic steel X6CrNiTi18-10. To this end, X-ray diffraction is used to determine the hoop and axial residual stresses on the outer and inner surfaces of the welded pipes. Measurements of the residual stresses and the radial distortion reveal that the thermal contraction of the weld and its vicinity are constrained by the tubular geometry, thus causing a characteristic residual stress state. Machining of the specimens influences the residual stress state on the surface through local plastic deformation and the introduction of machining residual stresses, which is shown by X-ray diffraction measurements after electrolytic polishing.

Keywords (IIW Thesaurus) Residual stresses · Austenitic stainless steels · Tubes and pipes

1 Introduction

The determination of residual stresses in welded structures and components is of great interest since residual stresses can have detrimental, but also beneficial effects on the structural performance, especially on the fatigue behavior. While significant progress has already been made in the numerical

computation of welding residual stresses, differences between numerical and experimental results, which are often observed as, e.g., in a recent round robin organized by the IIW [1], show the need of further research in this area.

This study is part of a research project which is dedicated to the application of advanced material models in simulations and their experimental validation. To this end, multi-pass girth-welded pipes of different steels are chosen because they reflect the constraining character of actual components much better than plane specimens. Numerical results and their comparison to experimental results will be subject of future work, whereas this study solely deals with the experimental residual stress analysis of austenitic steel pipes.

Based on numerical and experimental results, parametric studies of the residual stress development in girth-welded stainless steel pipes have been carried out by several authors, most notably by Brickstad and Josefson [2], Bouchard [3], and Song et al. [4], identifying the influence of several parameters on the through-thickness residual stress profiles within the pipe wall. An analytic approach based on shell theory presented recently by Song et al. [5] permits the prediction of through-thickness profiles at every location away from the weld, as well as the computation of the surface distribution of residual stresses. Apart from these comprehensive studies, numerous numerical and experimental investigations of the residual stress state in girth-welded pipes with particular pipe geometries and welding parameters can be found in the literature, e.g., [6–9]. The work of Deng and Murakawa [6] is of special interest, since stainless steel pipes of similar geometry and welding sequence are studied as in the present work, even though the wall thickness and heat input are lower there. The study at hand can also be compared to the authors' earlier contributions on the residual stress state in ferritic-pearlitic steel pipes of similar geometry [10, 11], where it has been shown that the governing mechanism of residual stress

Recommended for publication by Commission X-Structural Performances of Welded Joints - Fracture Avoidance

✉ Nico Hempel
n.hempel@tu-braunschweig.de

¹ Institute of Joining and Welding, TU Braunschweig, Langer Kamp 8, D-38106 Braunschweig, Germany

development is the thermal contraction of the weld, which causes pipe wall bending, and that phase transformation plays a minor role.

2 Experimental work

2.1 Characterization of the base material

Tensile tests were performed on specimens of X6CrNiTi18-10 with a circular cross section and a diameter of 5 mm, taken from the pipes in axial orientation. The tests were conducted according to ISO 6892-1 using an axial video extensometer.

2.2 Welding experiments

Tubular specimens of the austenitic steel X6CrNiTi18-10 (1.4541, AISI 321) with a geometry as shown in Fig. 1 were prepared. Therefore, the specimens were machined on the outer and inner surface in order to remove geometrical imperfections of the original pipes, resulting in an outer diameter of 114 mm and a wall thickness of 7.5 mm. As a weld preparation, a V-shaped groove was introduced at half-length, leaving a thin link between the two halves of the specimen in order to prevent misalignment and to guarantee well-defined clamping conditions. The link is molten during the welding process.

The specimens were metal active gas (MAG) welded with a filler wire of ISO 14343-A – G 19 9 Nb Si with a diameter of 1.2 mm using a shielding gas of 97.5 % Ar and 2.5 % CO₂. Welding was performed in flat position using a rotary table. Two passes were applied with a pulsed current, each at room temperature, resulting in nominal energy inputs of about 9 kJ/

cm for the root pass and 11 kJ/cm for the second pass. The welding parameters can be taken from Table 1. Both passes were welded in the same direction, the second pass being slightly offset circumferentially. Temperature measurements were performed in the vicinity of the weld at different axial and circumferential positions using Ni/CrNi thermocouples (type K).

After welding, micrographs were prepared in order to determine the microstructure and the hardness in the weld seam and the base material. The two-dimensional hardness distribution was determined by the ultrasonic contact impedance (UCI) method with a measuring point distance of 0.3 mm in both axial and radial direction of the pipe.

2.3 Residual stress analysis

The residual stresses in the vicinity of the welds were determined by X-ray diffraction (XRD). Residual strains were measured with an Ω -diffractometer by analyzing the shift of Mn-K α radiation interference lines originating from {311} lattice planes of the austenite. The diameter of the collimator was 2 mm. At each measuring point, interference lines were recorded at eight tilt angles ψ of 0°, 13°, 18°, 27°, 33°, 39°, 42°, and 45° in a 2θ interval of 145° to 159°. The shift of the interference line's center of gravity was analyzed with the $\sin^2\psi$ method and used to compute the residual strains, which in turn yielded the residual stresses by means of the X-ray elastic constants $s_1^{\{311\}} = -1.87 \cdot 10^{-6} \text{ mm}^2/\text{N}$ and $s_2^{\{311\}}/2 = 6.98 \cdot 10^{-6} \text{ mm}^2/\text{N}$. The theoretical penetration depth in steel using the experimental setup as outlined above is between 4.3 and 7.0 μm for Mn-K α radiation.

Fig. 1 Tubular specimen geometry

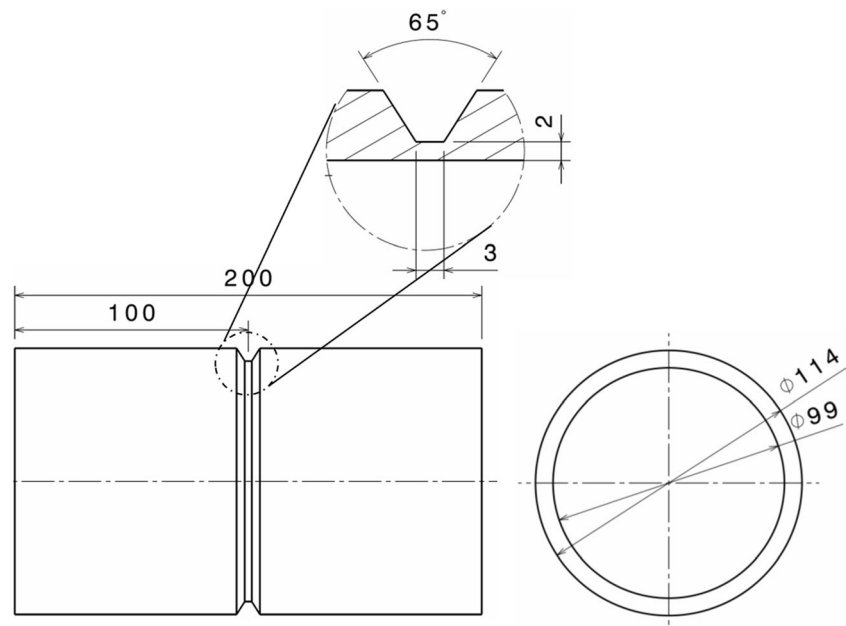
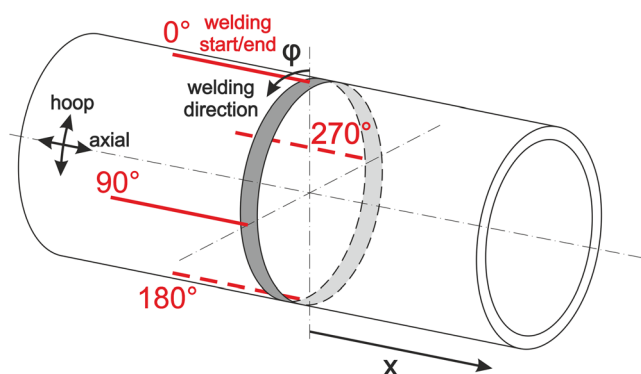


Table 1 Welding parameters for girth welds

Pass No.	Welding speed [cm/min]	Wire feed [m/min]	Ground time [ms]	Pulse time [ms]	Ground current [A]	Welding current [A]	Pulse voltage [V]	Welding voltage [V]	Heat input [kJ/cm]
1	28	4.9	6.1	2.0	70	163	32	22.9	9.1
2	32	6.8	2.8	2.0	70	225	32	24.5	11.2

The residual stresses were determined at points that were arranged along lines perpendicular to the welding direction. Both the longitudinal and the transverse residual stresses with respect to the welding direction, which are referred to as hoop and axial stresses, respectively, were studied within a range of up to 60 mm from the weld centerline. Due to the symmetry of the specimen and the weld the residual stresses were only determined on one side of the weld centerline. In the weld seam and the base metal close to the weld the distance between two measuring points was 1 mm due to the expected stress gradients in these areas. At a greater distance from the centerline measuring points were set every 2 to 5 mm. Measurements were taken on the inner and outer surfaces of the pipes at every 90° along the specimens' circumference, see Fig. 2. In this figure, a cylindrical coordinate system is introduced with the circumferential angle φ , marking welding start and welding direction, and the axial coordinate x that specifies the distance from the weld centerline. All measurements were taken in the negative x range.

The inner surfaces could only be accessed after sectioning the tubes into four quarters. To this end, the pipe was cut along lines parallel to the longitudinal axis, offset by 45° to the measuring lines. The residual stresses released by that process were monitored by strain gauge measurements on the inner surface as well as by repeated XRD measurements on the outer surface. In order to study the influence of the tubular geometry on the development of residual stresses, a strip of 6 mm width was cut from one of the quarters and residual stress analyses were performed on the outer surface. Additionally, the radial

**Fig. 2** Cylindrical coordinate system and locations of XRD measurements

distortion was determined by laser triangulation after welding and after each sectioning step.

In order to analyze the residual stress state across the depth near the outer surface, electrolytic polishing was used to remove thin layers of material from the surface. Therefore, the electrolytic polishing device LectroPol-5 and the electrolyte A2, both fabricated by the company Struers, were utilized. The removed material depth was mechanically determined using a digital gauge of 1 μm accuracy. Typically, between 10 and 50 μm were removed in an area of about $20 \times 10 \text{ mm}^2$ and XRD measurements were performed on the newly formed surface. These were not only used to compute the residual stresses, but also to qualitatively analyze the material condition on the current surface by determining the full width half maximum (FWHM) of the diffraction peaks. When material containing residual stresses is removed, a new equilibrium develops, thus altering the residual stress values in the remaining material. Mathematical correction methods exist for simple geometries and residual stress states, e.g., for a pipe with axially constant residual stresses where complete shells are removed, as given by Moore and Evans [12]. However, for the case considered here, a pipe with axial stress gradients where only a small portion of the surface is removed, no analytical correction methods exist. Moreover, the thickness of the removed layers is relatively small compared to the wall thickness, so that using no correction will only introduce small errors.

3 Experimental results and discussion

3.1 Characterization of the base material

The mean values of the most important mechanical parameters and the respective standard deviations computed from three tensile tests on X6CrNiTi18-10 specimens can be taken from Table 2.

Table 2 Mechanical parameters of X6CrNiTi18-10 as determined by the tensile tests

Yield strength at 0.2 % nonlinear strain (nominal)	Tensile strength (nominal)	Strain at fracture A_5 (nominal)
$222.9 \pm 6.7 \text{ MPa}$	$539.0 \pm 4.8 \text{ MPa}$	$57.32 \pm 0.08 \%$

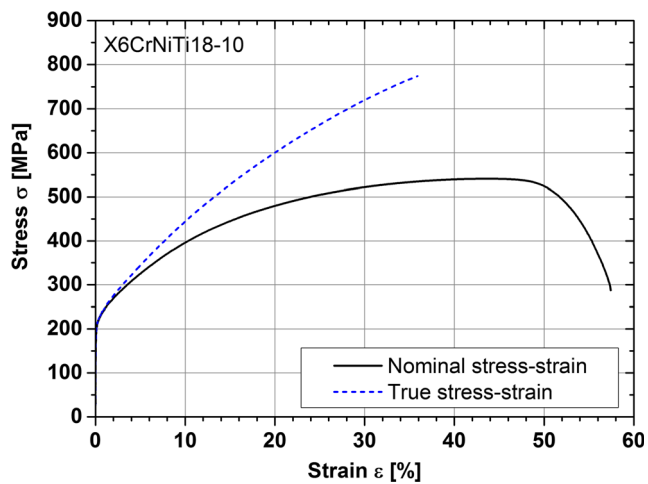


Fig. 3 Nominal and true stress-strain curves from tensile test of X6CrNiTi18-10

Both the nominal and the true stress-strain curves are shown in Fig. 3. It should be noted that the true stress-strain curve is only shown until the onset of necking since the actual cross section of the specimens has not been monitored directly. Due to the material's distinct ductility, high strain values can be attained until fracture, which is why the true stress-strain curve deviates significantly from the nominal one. The importance of this fact will be explained when the residual stress state is discussed.

3.2 Temperature measurements

Exemplarily, temperature is shown over time at different axial distances from the weld centerline in Fig. 4. The measurements were taken near $\varphi = 180^\circ$ on the outer surface of a pipe, which explains why higher temperatures were attained during welding of the second pass.

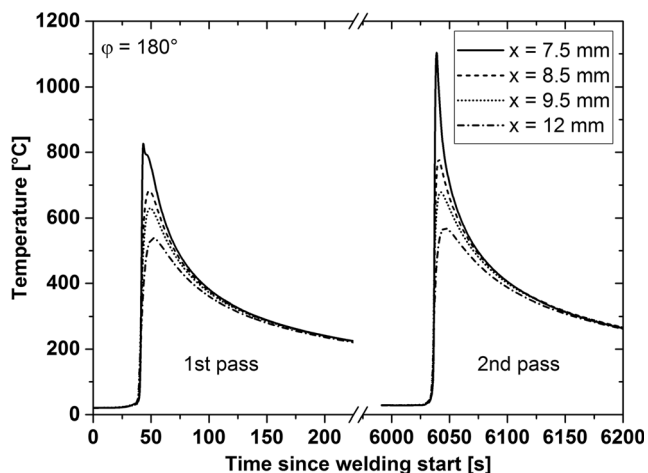


Fig. 4 Temperature over time at different axial positions for $\varphi = 180^\circ$, outer surface



Fig. 5 Micrograph taken from a tubular butt-weld at $\varphi = 135^\circ$

3.3 Characterization of the welded joints

Figure 5 shows a micrograph taken at a circumferential angle of $\varphi = 135^\circ$. The weld geometry with a distinct boundary between the base metal and the filler metal can be identified easily. The first welding pass is characterized by a pronounced weld root, a narrowing at about one third of the wall thickness and an almost linear broadening towards the outer surface of the pipe. The second pass is flat and wide at the top and features an argon finger which extends to about the middle of the wall thickness.

As expected for the high-alloy austenitic steel considered here, there is no classical HAZ as found in structural steels since allotropic phase transformation does not occur. This is confirmed by the hardness distribution shown in Fig. 6. As in the micrograph, the base and filler metal can be distinguished easily as both exhibit relatively homogeneous, but distinctly different hardness values. The hardness of the filler material is about 200 HV1, compared to 140 HV1 in the base metal.

3.4 Residual stress state at outer and inner surfaces of the pipes

The results of the XRD measurements taken at the inner and outer surfaces of a tubular specimen are shown in Figs. 7, 8, 9, and 10. The stress accuracy is exemplarily given for each measuring point at $\varphi = 180^\circ$.

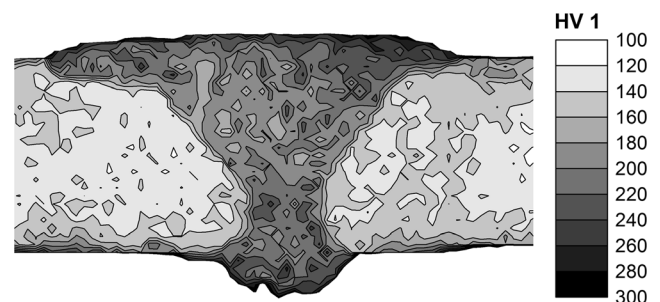


Fig. 6 Hardness distribution in the vicinity of a tubular butt-weld at $\varphi = 135^\circ$

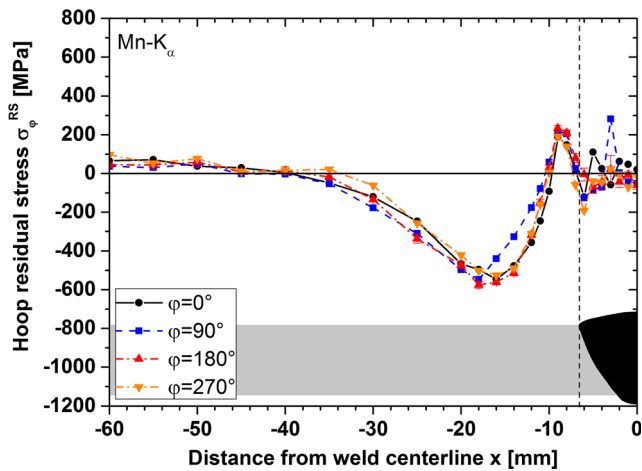


Fig. 7 Hoop residual stresses on the outer surface of an X6CrNiTi18-10 pipe

On the outer surface, the hoop residual stresses taken at different circumferential angles φ coincide relatively well, compared to the absolute values reached here, as can be seen in Fig. 7. They are about zero in the weld and reach a maximum of about 200 MPa close to the weld toe. At a distance of about 10 mm from the weld centerline (WCL), the stresses become compressive, featuring a minimum of -550 MPa at about 16 to 18 mm from the WCL. As the distance from the WCL becomes larger, the compressive stresses decrease and asymptotically approach a value of about 50 MPa.

The residual stresses on the inner surface could only be determined after sectioning the pipes. Here, the hoop residual stresses at different circumferential angles φ show a similar behavior as those on the outer surface, but their absolute values are higher, see Fig. 8. The hoop residual stresses are rather low in the weld but reach values of almost 800 MPa at 6 to 7 mm from the WCL, with the lowest maximum value at $\varphi = 0^\circ$. Again, the stresses then reach the compressive regime and show a minimum of -600 to -700 MPa at about 20 mm

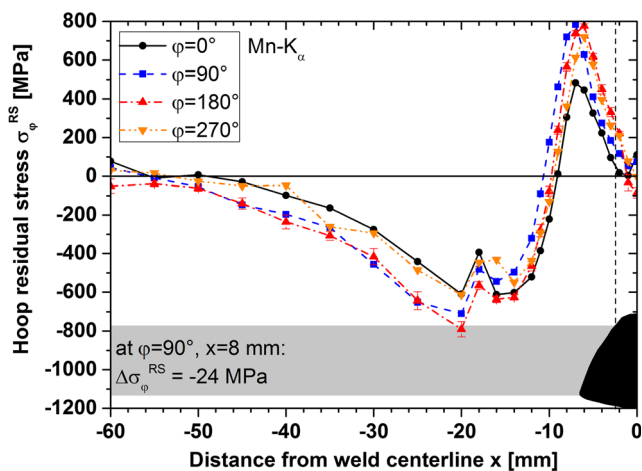


Fig. 8 Hoop residual stresses on the inner surface of an X6CrNiTi18-10 pipe after sectioning

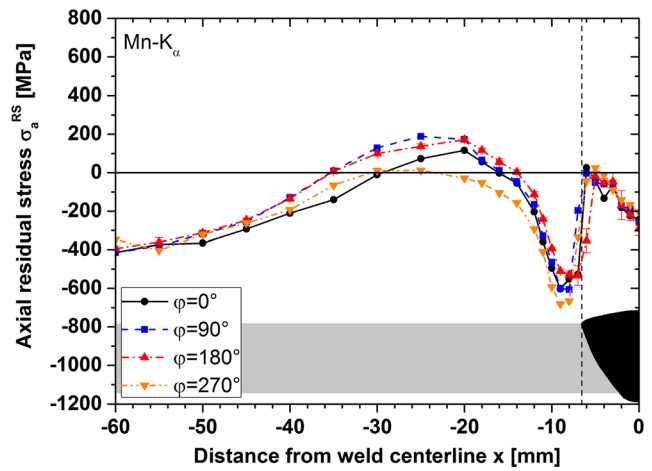


Fig. 9 Axial residual stresses on the outer surface of an X6CrNiTi18-10 pipe

from the WCL. In the area of the stress minimum, the stress curves are not smooth and exhibit a jump of about 200 MPa at all circumferential angles. This can be explained by an imperfection during the machining of the specimens and thus will not be considered in the discussion of the results. With increasing distance from the WCL, the compressive stresses decrease and are almost zero at distances higher than 50 mm from the WCL. It should be noted that sectioning the pipes had a small effect on the hoop residual stresses. Monitoring the strains released by the sectioning process revealed that about 24 MPa were released at $x = +8$ mm, which corresponds to the location of maximum residual stress, assuming symmetry about the WCL. The influence of sectioning on the residual stress state will be analyzed in more detail in a later section of this paper.

In axial direction, the residual stresses on the outer surface are rather low in the weld metal, especially close to the weld toe, see Fig. 9. Near the weld centerline, however, they are compressive, reaching values of about -200 MPa. A steep

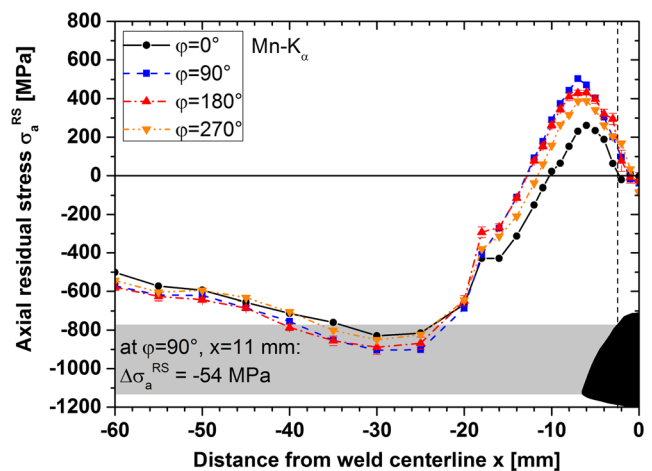


Fig. 10 Axial residual stresses on the inner surface of an X6CrNiTi18-10 pipe after sectioning

stress gradient can be found at the weld toe, resulting in highly compressive residual stresses of -550 to -700 MPa in the base metal. At larger distances from the WCL, the axial residual stresses first become tensile, with a maximum of about 200 MPa occurring at about 20 to 25 mm from the WCL, then re-enter the compressive regime and asymptotically approach a value of about -400 MPa.

On the inner surface, the axial residual stress curves show an opposite behavior, as depicted in Fig. 10. While the residual stresses in the weld are again very low, they take tensile values in the base material near the weld root, reaching a maximum of about 500 MPa at about 6 to 7 mm from the WCL. At $\varphi = 0^\circ$, the stress maximum is about 200 MPa lower than at the other circumferential angles. With increasing distance from the WCL, the residual stresses then become compressive and show a minimum of almost -900 MPa at 25 to 30 mm from the WCL. At even larger distances from the weld, the absolute stress values decrease again, but the curves stay in the compressive regime and do not exhibit an asymptotical behavior as observed in Figs. 7, 8, and 9. However, measurements at distances between 70 and 90 mm from the WCL, which are not shown in the figures, revealed that the axial residual stresses remain rather constant far away from the weld, taking values between -500 and -550 MPa. Again, sectioning influenced the residual stress state. A strain gauge applied to the inner surface at $x = +11$ mm indicated that the original axial residual stresses at this point were 54 MPa higher than after sectioning. As in the hoop direction, the stress curves exhibit a jump at $x = -18$ mm, which can also be attributed to an imperfection due to the turning process.

The results of the residual stress measurements presented in Figs. 7, 8, 9, and 10 can be interpreted in a consistent manner. Immediately after welding, the solidified weld metal as well as the heated zones of the base material contract during the cooling process. In longitudinal direction of the weld, i.e., in circumferential direction of the pipe, thermal contraction is strongly constrained by the adjoining base metal. Therefore, high compressive hoop residual stresses can be observed in the base metal both on the inner and on the outer surfaces between 10 and 40 to 50 mm from the WCL, see Figs. 7 and 8. In turn, tensile hoop residual stresses would be expected in the weld, which is not confirmed by the measurements. A possible explanation for this effect is the fact that XRD measurements in steel only take the material volume, and thereby the residual stresses, in the first few micrometers near the surface into account. In the weld, the measured values are therefore taken from the weld reinforcement, which is subject to a lower constraint as there is no base material in the immediate vicinity, which may be the reason why no tensile residual stresses are found here. The fact that the residual stresses in the highly heated base material close to the weld toe are tensile and rapidly fall off towards the weld, see Fig. 7, support this thesis.

Due to the self-constraining geometry of the pipe, the thermal contraction of the weld also has a pronounced effect on the axial residual stress distribution. The circumferential contraction causes necking of the pipe and thus bending of the pipe wall due to the radial displacement of the weld, which can also be seen in deformation measurements using laser triangulation that are shown in Fig. 13 and will be treated in more detail in the next section. Consequently, the axial residual stresses are characterized by a bending stress state. On the outer surface, the material is compressed in the vicinity of the weld and stretched at a distance of $|x| > 16$ mm due to the curvature of the pipe wall, causing compressive and tensile residual stresses, respectively, as shown in Fig. 9. Typical of bending, this pattern is reversed on the inner surface of the pipe, where the axial residual stresses are tensile near the weld seam and compressive for $|x| > 14$ mm, see Fig. 10. In the weld, the residual stress values are lower, which can again be attributed to the fact that only the near-surface residual stresses have been measured and that the weld reinforcement is not affected by the wall bending as much as the base material. Moreover, the weld also contracts in axial direction during cooling, causing tensile stresses which are superposed with the bending stresses. This helps to explain why the high compressive stresses near the weld toe on the outer surface vanish rapidly in the weld metal, as can be seen in Fig. 9.

The pronounced influence of pipe wall bending on the residual stress state in girth-welded pipes has also been noted by other authors. According to Bouchard and Song et al. the bending influence on the axial residual stresses increases with the heat input [3, 4]. Therefore, it can be inferred that the heat input used in this study is relatively high. Deng and Murakawa also observed a strong bending influence in their work on a pipe weld of similar geometry [6].

Far away from the weld, both on the inner and on the outer surfaces, highly compressive axial residual stresses of -400 to -550 MPa occur, even though the thermal and mechanical influence of the weld should be minimal at a distance of 60 mm from the WCL. The likeliest explanation for this phenomenon is the machining process of the specimens, during which residual stresses may be introduced. This assumption was confirmed by measurements on unwelded specimens, which also showed significant residual stresses, especially in the axial direction of the pipes. The steel X6CrNiTi18-10 is well known for its proneness to near-surface plastic deformation during machining, which can cause residual stresses. Since the X-rays only penetrate the first few micrometers from the surface, the machining residual stresses are fully taken into account in the measurements presented here and are thus superposed with the welding residual stresses. However, the machining residual stresses, which can be assumed as constant over the specimen length after the turning process, cannot simply be subtracted from the total residual stress state. It can be inferred that welding alters the machining residual

stresses since it can be considered as a local heat treatment, causing recrystallization and a local reduction of the yield strength. Therefore, it is assumed that the influence of the machining process fades as the distance from the WCL decreases, i.e., as the maximum temperature during welding increases. This will be investigated in a later section of this paper, using electrolytic polishing.

Plastic deformation of the steel X6CrNiTi18-10 is also accompanied by substantial mechanical hardening, as shown in Fig. 3. Therefore, very high residual stress values can be found in the pipes investigated here which even surpass the nominal tensile strength. This is possible since XRD detects the true residual stresses, which is why the true stress-strain curve should be used as a reference. Again, it should be noted that the true stress-strain curve depicted in Fig. 3 was only recorded until the onset of necking. Thus, even higher stress values than the maximum of this curve can be reached. For instance, the compressive axial residual stresses on the inner surface take values of almost -900 MPa. Compared to a similar study [6], the residual stress values determined on the surface seem overly high. Therefore, the residual stresses will be analyzed again after a thin surface layer has been removed by electrolytic polishing, which will be the focus of a later section of this paper.

At different circumferential angles, variations of the residual stresses of up to 200 MPa were found. The fact that the absolute residual stress values are lower for $\varphi = 0^\circ$ may be due to effects of the welding start and stop, which was also observed by Deng and Murakawa [6]. While the origin of the other variations remains unclear, it is inferred that their high magnitude also results from the pronounced work hardening effect, leading to generally very high residual stress values. As the variations are relatively small compared to these high absolute values, a nearly axisymmetric residual stress state can be assumed.

Comparing the results of the residual stress measurements on austenitic X6CrNiTi18-10 pipes with studies on girth-welded pipes of the ferritic-pearlitic steel S355J2H+N with a similar geometry [10, 11] yields some interesting remarks on the latter works. While it has already been demonstrated that the governing mechanism causing residual stresses in the S355J2H+N pipes was thermal contraction and pipe wall bending, these conclusions can be confirmed by the present paper. Despite the large quantitative differences between the results obtained in the two materials, the residual stress distributions are qualitatively almost the same, even though phase transformations occur in S355J2H+N, but not in X6CrNiTi18-10, confirming that this mechanism played a minor role in the residual stress development in the S355J2H+N pipes. However, the conclusion that the local maxima of the hoop residual stresses on the outer surface of these pipes, occurring in the heat-affected zone near the weld toe, arise from phase transformations [10, 11], has to be

revised. The fact that these maxima also occur in the X6CrNiTi18-10 pipes, see Fig. 7, suggests a mechanical origin, possibly in the hindered contraction of the highly heated base material in this zone. Quantitatively, the residual stresses found in the welded X6CrNiTi18-10 pipes are generally higher than those in the S355J2H+N pipes due to the work hardening effect on the surface described above.

3.5 Residual stress and deformation analysis of sectioned pipes

In order to analyze the effect of sectioning the pipes, which is a necessity for taking XRD measurements on the inner surface, as well as to investigate the influence of the self-constraining tubular geometry on the residual stress state, a pipe is first cut into quarters, then into a strip of 6 mm width. The hoop and axial residual stresses at $\varphi = 90^\circ$ on the outer surface before and after each sectioning step are measured by XRD and depicted in Figs. 11 and 12. Additionally, the radial deformation was determined on the outer surface using laser triangulation, see Fig. 13.

Both the hoop and the axial residual stresses are hardly affected by cutting the pipe into quarters. Apart from the axial residual stress minimum at the weld toe, whose absolute value is about 150 MPa lower after sectioning, see Fig. 12, the curves are nearly identical. These results are confirmed by the deformation measurements which revealed that the surface geometry of the pipe did not change by cutting it into quarters, as can be seen in Fig. 13. Both the unsectioned pipe and the quarter pipe show the pronounced pipe wall bending associated with the circumferential contraction of the weld, which is the main mechanism for causing residual stresses, as outlined in the previous section. Thus, it can be concluded that no significant amount of residual stresses has been released by elastic recovery of the original shape of the unwelded pipe. These results are in agreement with the strain gauge

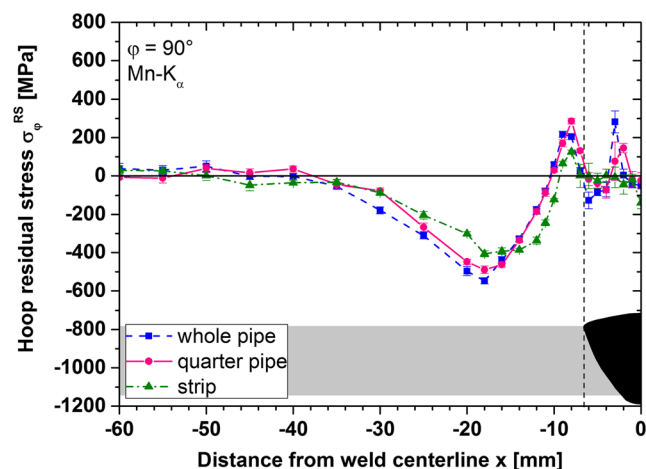


Fig. 11 Hoop residual stresses at $\varphi = 90^\circ$ on the outer surface of an X6CrNiTi18-10 pipe before and after sectioning

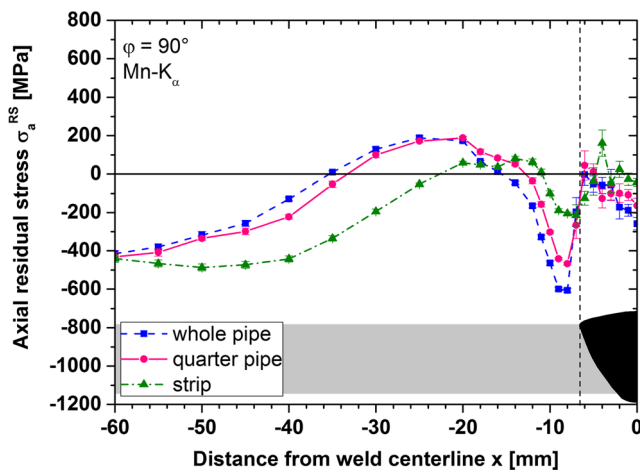


Fig. 12 Axial residual stresses at $\varphi = 90^\circ$ on the outer surface of an X6CrNiTi18-10 pipe before and after sectioning

measurements taken during cutting the pipe into quarters, which were already mentioned in the previous section. Here, only low amounts of strains were released due to cutting, the axial direction being slightly more affected than the hoop direction.

The situation changes after further cutting the pipe into a small strip of 6 mm width, thereby virtually removing the tubular geometry of the specimen. In hoop direction, the residual stress change is relatively small, as depicted in Fig. 11. The maximum absolute value of the compressive stresses in the base material is about 100 MPa lower than in the uncut specimen, whereas the maximum near the weld toe has decreased by about 50 MPa. In axial direction, however, the residual stress curve clearly differs from the ones taken from the unsectioned or quarter pipe, as shown in Fig. 12. Most noticeably, the residual stress minimum at the weld toe has diminished significantly; only -200 MPa remain in the specimen. Moreover, between 20 and 55 mm from the WCL, the

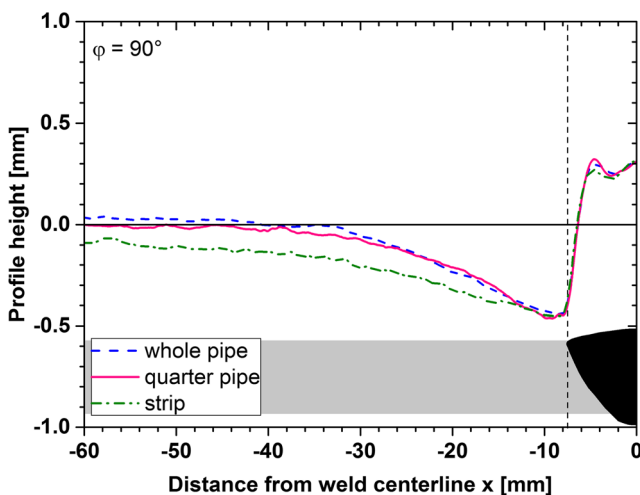


Fig. 13 Surface profiles at $\varphi = 90^\circ$ on the outer surface of an X6CrNiTi18-10 pipe before and after sectioning, determined by laser triangulation

residual stress curve has been shifted downwards, thus mainly being in the compressive regime. The largest difference can be found between 30 and 40 mm from the WCL, where the residual stresses are up to 340 MPa lower than in the unsectioned pipe. At a distance of 60 mm from the WCL, however, the residual stresses determined in the unsectioned pipe, the quarter pipe and the strip are the same.

The large shift can be interpreted as an elastic release of the axial residual stresses as the self-constraining tubular geometry is removed by sectioning the pipe into a small strip. This assumption is in agreement with the deformation measurements presented in Fig. 13, which shows that the base material of the small pipe strip is bent downwards about the weld seam, thereby releasing the axial residual stresses. This underlines that this stress component is mainly influenced by pipe wall bending due to the tubular constraints. However, a certain curvature, i.e. wall bending, can still be observed in the strip, indicating that plastic deformation of the pipe must have occurred.

3.6 Residual stress analysis in deeper material layers using electrolytic polishing

In this part of the study, electrolytic polishing is used to remove thin layers of material from the surface in order to analyze the residual stress state below the original surface. In total, three areas of about $20 \times 10 \text{ mm}^2$ were subjected to electrolytic polishing and the residual stresses were measured in windows ranging from 0 to 16 mm, from 25 to 40 mm and from 70 to 85 mm from the WCL, respectively.

Figures 14 and 15 show the hoop and axial residual stresses on the surface and after removing 200 and 420 μm of material, respectively; the steps in between are not shown for the purpose of clarity. The scale of the vertical axis has been adjusted in order to emphasize changes of the residual stresses. The hoop and axial residual stresses on the surface of this

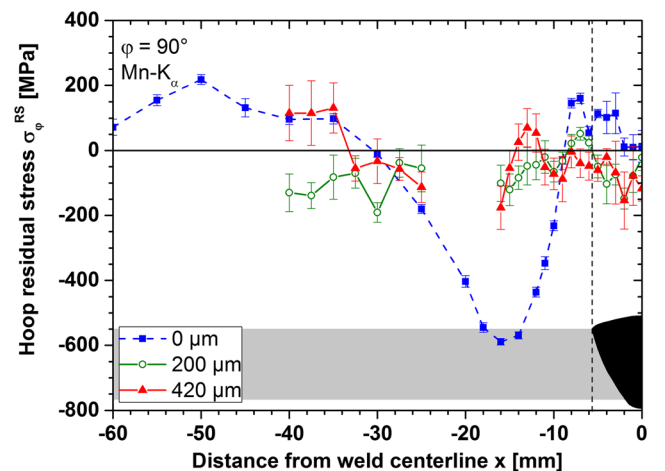


Fig. 14 Hoop residual stresses at $\varphi = 90^\circ$ on the outer surface, at 200 μm and at 420 μm depth

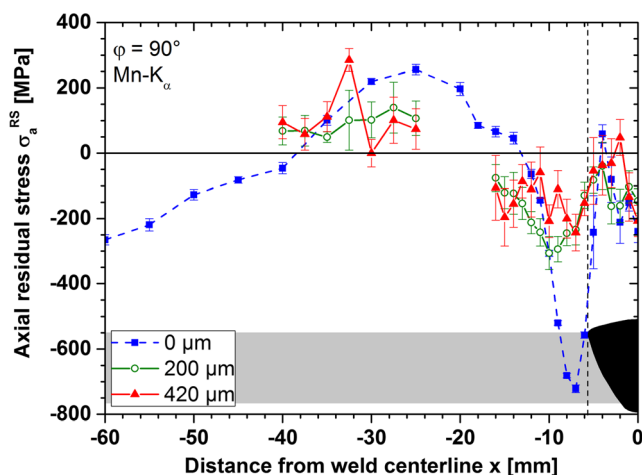


Fig. 15 Axial residual stresses at $\varphi = 90^\circ$ on the outer surface, at 200 μm and at 420 μm depth

specimen, represented by the blue curves, are distributed in the same characteristic way as already seen in Figs. 7 and 9. However, the machining residual stresses measured at distances larger than 60 mm from the WCL are different here, reaching tensile 120 MPa in the hoop direction and compressive values of about -260 MPa in the axial direction. The variation of the machining residual stresses from one specimen to another can be explained by the fact that the machining parameters were neither prescribed nor monitored, which does not affect the generality of this study regarding the interaction of welding and machining residual stresses.

In the weld, both hoop and axial residual stresses vary only slightly across the depth, as can be seen in Figs. 14 and 15, whereas significant differences are found in the base material. At the location where the hoop residual stresses exhibit a minimum of -600 MPa on the surface, only about -120 MPa are found at 200 μm depth, see Fig. 14. Near the weld toe, the stress maximum has decreased from 160 to 50 MPa, whereas the stresses at about 40 mm from the WCL have reversed their sign. The results taken from a depth of 420 μm do not differ significantly from those at 200 μm , except for the fact that tensile residual stresses instead of compressive ones are found at about 40 mm from the WCL. It should be noted that the measurement uncertainty generally increases at larger depths, as reflected by the length of the error bars in Figs. 14 and 15.

In axial direction, a similar behavior can be observed. The distinct minimum of the axial residual stresses at the weld toe diminishes with increasing depth, see Fig. 15. While the residual stresses reached almost -750 MPa on the surface, only -300 MPa and -240 MPa are determined at depths of 200 and 420 μm , respectively. The maximum of the axial residual stress at about 25 mm from the WCL seems to be shifted farther away from the weld.

The residual stresses determined near the specimen end at about 80 mm from the WCL are not shown in the figures.

Here, hoop residual stresses of 120 MPa have been found at the surface, whereas measurements after electrolytic polishing revealed values of -170 and -20 MPa at depths of 200 and 420 μm , respectively. In axial direction, the compressive residual stresses decrease gradually from -260 MPa at the surface to -190 MPa at 200 μm and to -90 MPa at 420 μm .

The results shown in Figs. 14 and 15 can be interpreted more easily by studying the full width half maximum (FWHM) of the X-ray diffraction peaks at different depths from the surface. The FWHM is a characteristic quantity describing the diffraction peak shape and allows conclusions about the material conditions, e.g., about the grain size and the dislocation density, which is a measure of plastic deformation. While a more detailed analysis, see e.g. [13], is out of the scope of this study, the raw FWHM curves plotted against the distance from the WCL for different depths after electrolytic polishing, as shown in Fig. 16, can already be very insightful.

On the outer surface of the pipe, i.e., at a depth of 0 μm , the FWHM slowly decreases from 3.5° at a distance of 60 mm from the WCL to 3.4° at $x = -30$ mm, then decreases slightly more quickly until reaching 3.0° at $x = -8$ mm, before quickly dropping to about 2.0° in the weld. With increasing depth, the FWHM in the base material gradually decreases until reaching values below 1.8° at a depth of 200 μm . The FWHM then remains almost constant for subsequent polishing steps. In the weld, the FWHM also drops to about 1.8° after the first polishing step, then remains at that level for any further step. At depths larger than 30 μm and below 420 μm , a small maximum of the FWHM can be observed in the base material near the weld toe.

The large FWHM on the outer surface can be explained by the machining of the tubular specimens, leading to considerable plastic deformation and thus work hardening in near-surface zones of the material. As deeper material layers are less affected by plastic deformation, the FWHM gradually

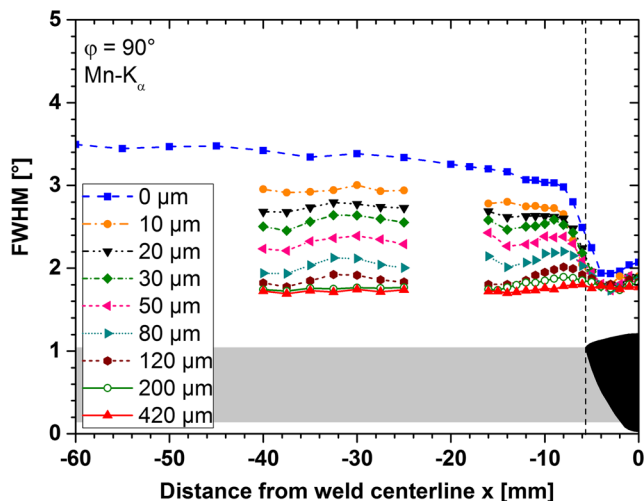


Fig. 16 Full width at half maximum of diffraction peaks at $\varphi = 90^\circ$ in different depths near the outer surface of an X6CrNiTi18-10 pipe

decreases with increasing depth. This effect tapers off, which can be seen by the fact that the FWHM asymptotically approaches values of about 1.8° , which are reached at a depth of 200 μm .

The slow decrease of the FWHM on the outer surface as the weld is approached can be interpreted as a heat treatment effect, caused by the elevated temperatures reached during or directly after welding. Thus, the machining influence may be mitigated through recrystallization or facilitated dislocation motion. However, temperature measurements in the vicinity of the weld, as shown in Fig. 4, suggest that significant temperature effects are supposedly limited to areas very close to the weld. While temperatures of 1100 $^\circ\text{C}$ were reached at 7.5 mm from the WCL, only 550 $^\circ\text{C}$ were measured at 12 mm distance.

Within the weld, the FWHM is rather low. Here, a cast structure develops when the weld metal solidifies, without significant plastic deformation at the surface as in the base material. Therefore, the FWHM remains constant across the depth. The small drop after the first polishing step may be explained by an oxide layer covering the weld, which is instantly removed when electrolytic polishing is applied.

With the FWHM results shown in Fig. 16 in mind, the changes of the residual stress curves across the depth, as seen in Figs. 14 and 15, can be interpreted. Such a large variation of the residual stresses within only 200 μm cannot simply be explained by the change of the welding residual stresses across the depth, which may of course exist but is expected to be much lower. Two other effects mainly influence the residual stress distribution near the surface. Firstly, machining induces significant plastic deformation and thus work hardening of the near-surface material. This effect rapidly decreases across the depth as qualitatively shown by the FWHM curves in Fig. 16. Thereby, the pronounced decrease of the absolute maximum stress values across the depth, as seen in Figs. 14 and 15, can easily be explained. The plastically deformed material on the specimen surface allows for very high residual stress values due to the distinct increase of the yield strength caused by work hardening. When the highly deformed material is removed, lower residual stresses are found since the yield strength is lower in material layers below the surface.

Secondly, residual stresses arising from the machining process of the specimens or, more generally, from the fabrication process of the pipes are non-uniformly distributed across the depth and are superposed with the welding residual stresses. It should be noted that the former stresses are still non-zero at a depth of 420 μm as revealed by measurements far away from the weld, i.e., about 80 mm from the WCL. Therefore, it can be assumed that the results shown in Figs. 14 and 15 are still affected by the fabrication residual stresses and thus do not show the pure welding residual stresses. Furthermore, the residual stress values determined after electrolytic polishing should be used with care. As explained at the beginning of

this paper, these values reflect a new equilibrium established after removing stressed material and have not been corrected mathematically. Thus, more research is necessary to analyze the residual stress state at higher depths, e.g., by using neutron diffraction.

Near the weld toe, a minimum axial residual stress of -300 MPa is found at a depth of 200 μm , whose absolute value is higher than the yield strength as determined in the tensile tests, see Table 2. As the FWHM curves indicate that the influence of the surface work hardening is minimal at this depth, it is inferred that plastic deformation has occurred near the weld toe, which would explain the remaining curvature of the small strip cut from a pipe shown in Fig. 13. This conclusion is supported by the fact that the FWHM curves at depths between 30 and 200 μm exhibit a small maximum near the weld toe, see Fig. 16, which indicates plastic deformation.

4 Summary and conclusions

The residual stress state on the inner and outer surfaces of butt-welded pipes of the austenitic steel X6CrNiTi18-10 has been investigated by X-ray diffraction, complemented by sectioning and electrolytic polishing. The main conclusions are summarized in the following:

- Welding residual stresses in the X6CrNiTi18-10 pipes are caused by the thermal contraction of the weld and its vicinity.
- The circumferential contraction of the weld zone leads to significant necking of the pipe, thereby causing wall bending and a distinct axial residual stress state. The axial residual stresses take high compressive values near the weld toe and high tensile values near the weld root. It is thus inferred that the weld root is more susceptible to fatigue crack initiation.
- Sectioning the pipes into quarters for taking measurements on the inner surface has a relatively low effect on the surface residual stress state. The axial component is influenced to a higher extent than the hoop component, which can be explained by the tubular geometry being disturbed by cutting the pipe. This holds especially for sectioning the pipe into a small strip, thus highlighting the wall bending influence on the axial residual stresses.
- When machining residual stresses are present in a component, the surface residual stress state can be rather complex since both welding and machining residual stresses are usually non-constant in the vicinity of a weld and are barely separable from each other as they merge to a resulting residual stress state. Electrolytic polishing can be used to remove the material surface, but machining residual stresses were still present at a certain depth in this

work, thus complicating the analysis of the welding residual stresses.

- Machining can also cause considerable plastic deformation and hardening of the material on the surface, which may lead to higher surface residual stress values. Again, electrolytic polishing may be used to remove material from the surface in order to analyze the welding residual stresses under original material conditions.
- The welding residual stresses found in the austenitic X6CrNiTi18-10 steel pipes investigated in this paper confirm the conclusions about the residual stress development in the ferritic-pearlitic S355J2H+N steel pipes drawn from previous studies [10, 11].

Acknowledgments We would like to thank the German Federation of Industrial Research Associations (AiF) for their financial support of the research project IGF No. 17.619N. This project was carried out under the auspices of AiF and financed within the budget of the Federal Ministry for Economic Affairs and Energy through the program to promote joint industrial research and development (IGF).

The authors also would like to thank BASF SE, Ludwigshafen, Germany, for the allocation of X6CrNiTi18-10 pipes, which were used for this study.

References

1. Wohlfahrt H, Nitschke-Pagel T, Dilger K, Siegele D, Brand M, Sakkietitubtra J, Loose T (2012) Residual stress calculations and measurements – review and assessment of the IIW round robin results. *Weld World* 56(09/10):120–140
2. Brickstad B, Josefson BL (1998) A parametric study of residual stresses in multi-pass butt-welded stainless steel pipes. *Int J Pres Ves Pip* 75:11–25
3. Bouchard PJ (2007) Validated residual stress profiles for fracture assessments of stainless steel pipe girth welds. *Int J Pres Ves Pip* 84: 195–222
4. Son S, Dong P, Pei X (2015) A full-field residual stress estimation scheme for fitness-for-service assessment of pipe girth welds: part I – identification of key parameters. *Int J Pres Ves Pip*. 126-127:58–70
5. Song S, Dong P, Pei X (2015) A full-field residual stress estimation scheme for fitness-for-service assessment of pipe girth welds: part II – a shell theory based implementation. *Int J Pres Ves Pip*. 128:8–17
6. Deng D, Murakawa H (2006) Numerical simulation of temperature field and residual stress in multi-pass welds in stainless steel pipe and comparison with experimental measurements. *Comp Mater Sci* 37:269–277
7. Deng D, Murakawa H, Liang W (2008) Numerical and experimental investigations on welding residual stress in multi-pass butt-welded austenitic stainless steel pipe. *Comp Mater Sci* 42:234–244
8. Yaghi AH, Hyde TH, Becker AA, Sun W, Williams JA (2006) Residual stress simulation in thin and thick-walled stainless steel pipe welds including pipe diameter effects. *Int J Pres Ves Pip*. 83: 864–874
9. Yaghi AH, Hyde TH, Becker AA, Sun W, Hilson G, Simandjuntak S, Flewitt PEJ, Pavier MJ, Smith DJ (2010) A comparison between measured and modeled residual stresses in a circumferentially butt-welded P91 steel pipe. *J Press Vessel Technol* 132:011206
10. Hempel N, Nitschke-Pagel T, Dilger K (2014) Residual stresses in multi-pass butt-welded tubular joints. *Adv Mat Res* 996:488–493
11. Hempel N, Nitschke-Pagel T, Dilger K (2015) Residual stresses in multi-pass butt-welded ferritic-pearlitic steel pipes. *Weld World* 59(4):555–563
12. Moore MG, Evans WP (1958) Mathematical correction for stress in removed layers in X-ray diffraction residual stress analysis. *SAE Trans* 66:340–345
13. Klug HP, Alexander LE (1974) X-ray diffraction procedures: for polycrystalline and amorphous materials, 2nd edn. Wiley, New York